



HAL
open science

Optically active cross-band transition in double-walled carbon nanotube and its impact on Raman resonances

M. Paillet, V.N. Popov, H.N. Tran, J.-C. Blancon, D.I. Levshov, R. Arenal, R. Parret, A. Ayari, A. San Miguel, F. Vallée, et al.

► To cite this version:

M. Paillet, V.N. Popov, H.N. Tran, J.-C. Blancon, D.I. Levshov, et al.. Optically active cross-band transition in double-walled carbon nanotube and its impact on Raman resonances. *Carbon*, 2022, 196, pp.950-960. 10.1016/j.carbon.2022.05.044 . hal-03762978

HAL Id: hal-03762978

<https://hal.science/hal-03762978>

Submitted on 29 Aug 2022

HAL is a multi-disciplinary open access archive for the deposit and dissemination of scientific research documents, whether they are published or not. The documents may come from teaching and research institutions in France or abroad, or from public or private research centers.

L'archive ouverte pluridisciplinaire **HAL**, est destinée au dépôt et à la diffusion de documents scientifiques de niveau recherche, publiés ou non, émanant des établissements d'enseignement et de recherche français ou étrangers, des laboratoires publics ou privés.

Optically active cross-band transition in double-walled carbon nanotube and its impact on Raman resonances

M. Paillet,^{1,*} V.N. Popov,² H. N. Tran,¹ J.-C. Blancon,³ D. I. Levshov,^{1,#} R. Arenal,^{4,5,6} R. Parret,^{1,##} A. Ayari,³ A. San Miguel,³ F. Vallée,³ N. Del Fatti,³ A. A. Zahab,¹ J.-L. Sauvajol¹

¹Laboratoire Charles Coulomb (UMR5221), CNRS-Université de Montpellier, F-34095 Montpellier, France

²Faculty of Physics, University of Sofia, BG-1164 Sofia, Bulgaria

³Institut Lumière Matière, UMR5306 Université Lyon 1-CNRS, Université de Lyon F-69622 Villeurbanne cedex, France

⁴Laboratorio de Microscopias Avanzadas (LMA), Universidad de Zaragoza, Mariano Esquillor s/n, 50018 Zaragoza, Spain.

⁵Instituto de Nanociencia y Materiales de Aragon (INMA), CSIC-U. de Zaragoza, Calle Pedro Cerbuna 12, 50009 Zaragoza, Spain.

⁶ARAID Foundation, 50018 Zaragoza, Spain.

*Corresponding author. Tel: +33-467143539. E-mail: matthieu.paillet@umontpellier.fr

#Current address: University of Antwerp, Department of Physics, Universiteitsplein 1, B-2610 Antwerpen, Belgium

##Current address: Aix Marseille Université, CNRS, CINAM, UMR 7325, Campus de Luminy, 13288, Marseille, France

Abstract

Double-walled carbon nanotubes (DWNTs), often regarded as the simplest one-dimensional (1D) van der Waals moiré superlattices, are the ideal structures to explore the interlayer coupling, including mechanical and electronical coupling, at the nanoscale in 1D systems. By

combining spatial modulation spectroscopy (SMS) and resonant Raman scattering (RRS) experiments on well-identified individual free-standing DWNTs with the calculations of their optical absorption by using the recursion method with non-orthogonal tight-binding (NTB) basis functions, we are able to unambiguously assign the nature, namely mirror transition or cross transition, of each optical transitions in DWNTs. Our study identifies and allows to determine the conditions of the mixing of the electronic states leading to the appearance of cross transitions in the optical absorption of DWNTs, beyond of the so-called Koshino's criteria previously derived. On the other hand, the striking behavior of the resonant excitation profile (REP) of the Raman active modes around the cross transition reveals the strong sensitivity of the modes intensity on the electronic interlayer coupling in DWNTs, emphasizing the relevance of Raman spectroscopy for studying the electronic and mechanical coupling at the nanoscale.

1. Introduction

When repetitive structure are overlaid against each other a new superimposed moiré pattern emerges. In layered two-dimensional (2D) van der Waals-coupled heterostructures, engineering of the electronic band structure through the formation of moiré superlattice can lead to significant alternation of the electronic properties of such nanostructures. This is exemplified in twisted bilayer graphene (t-BLG) where a weak van der Waals interlayer coupling between 2D layers alters the electronic structure of each layer and induces van Hove singularities (VHs) in the electronic density of states of t-BLG, the position of VHs depending on the twist angle between the layers (see Ref. [1] and references therein).

Double-walled carbon nanotubes (DWNTs) are often regarded as the simplest one-dimensional (1D) van der Waals moiré superlattices, being the ideal structures to explore the interlayer coupling at the nanoscale in 1D systems [2,3]. DWNTs possess a unique two-layer

coaxial structure consisting of two nested single-walled carbon nanotubes (SWNTs) bound together by weak van der Waals interactions. Indeed the electronic, mechanical, optical and vibrational properties of DWNTs are not only inherited from their SWNTs building blocks but also result from interlayer interactions [3-21].

DWNTs are uniquely defined by the chiral indices (n_i, m_i) and (n_o, m_o) of their inner and outer SWNTs (or “layers”), respectively and afterward they are denoted as $(n_i, m_i)@ (n_o, m_o)$. Structurally speaking, the majority of DWNTs are incommensurate (a DWNT structure is commensurate if the two constituents SWNTs have a common periodicity along its axis and such a situation is very exceptional). The incommensurability together with the curved geometry and structural diversity of DWNTs result in interesting electronic and optical properties offering opportunities for the development of applications [22-26].

Studying the carbon nanotubes at an individual level constitutes the best approach to correlate their structural characteristics to their physical properties. This assertion is even more relevant for DWNTs. Indeed, even mild ultrasonication, the method almost always used to disperse DWNTs from powders to obtain individualized nanotubes suspensions, has been found to easily extract the inner SWNTs from outers [27-29]. Such samples are consequently actually constituted, at best, of a mix of SWNTs and DWNTs. This now widely accepted fact severely complicates DWNTs spectroscopic studies and even questions the interpretations of the results obtained on such “DWNTs” suspensions. During the past decade, several spectroscopy-based methods have been developed to probe the electronic and optical properties of identified SWNTs at the single nanotube level, such as Rayleigh scattering [30-34], resonant excitation profile (REP) of Raman active modes [35], photoluminescence [36-37], and absorption-based techniques [35,37-44]. More recently, such approaches have been used to explore the properties of individual well-identified DWNTs. It was experimentally established that electronic [8,9,17] and vibrational [4,6,7,10,12,15,16] properties differ from those of their constituent SWNTs due

to interlayer coupling effects. Concerning the electronic and optical properties a pioneer work [9] has put in evidence a one-to-one correspondence between the optical transitions of the DWNTs and those from the constituents SWNTs, but the transition energies are always shifted varying from a redshift of about 190 meV to a blueshift of 50 meV in different incommensurate DWNT species. These results were understood as due to the hybridizing of the electronic states of the inner and outer nanotubes, and the resulting chirality-dependent interlayer coupling was described in the framework of an one-dimensional zone-folding of the electronic structure of twisted and stretched graphene bilayers [9]. An alternative approach, overlapping in part that of the Ref. [9], showed that, dependent on the DWNT structure, a significant alteration of electronic bands can occur and the resulting optical spectrum can be far from a simple sum of the SWNT spectra [11]. Drastic changes of the electronic bands are predicted when two conditions are fulfilled (the so-called Koshino's criteria): (i) either the chiral vectors directions for the inner and outer SWNTs are close to each other and (ii) the chiral vectors difference is parallel either to the armchair direction for the so-called strong-coupling regime, or to the zigzag direction for the so-called flatband or localized insulating regime [11]. Outside of these criteria, it is expected that the interaction between the walls should be very weak [11,20]. It was also noted that the intertube distance plays a key role, *i.e.* the shorter the distance, the stronger the interactions [3,11,20]. Recently, a drastic change of the optical transition spectrum in (12,11)@(17,16) DWNT was experimentally observed [17] and explained as resulting of strong interlayer coupling effects as expected from Koshino's criteria in this peculiar DWNT formed by two-nearly armchair SWNTs [10]. More recently, a linear relation between the optical transition energy and frequency shifts of the inner tube RBLM has been established within the same theoretical background and verified experimentally on DWNTs suspensions only [20]. Nonetheless, it has been found that the photoluminescence of inner tubes was quenched by 4 orders of magnitude for "weakly interacting" DWNTs pointing out an efficient energy transfer

from inner to outer layer even in such cases [14]. Furthermore, two theoretical works have revisited the effects of the interlayer coupling on the optical spectra of DWNTs. In a first study, using the tight-binding approximation, the authors demonstrate that in specific DWNTs the interlayer coupling can slightly modify the electronic band structure of pristine nanotubes in such a way that unconventional inter-tube electronic transitions become possible creating additional peaks in the DWNT optical spectrum [18]. In a second study, the optical absorption of DWNTs was calculated using the recursion method with non-orthogonal tight-binding (NTB) basis functions [19]. The recursion method is used with ab-initio derived NTB parameters, which yields realistic prediction of the optical transitions of layered carbon structures and permits addressing their physical origin. Calculations reveal that the interlayer interaction can give rise to major changes of the electronic structure. This theoretical work extends the previous ones by identifying the conditions and effects of the mixing of the electronic states on the optical response of DWNTs:

- (i) Strong mixing of the electronic states can occur if the two non-interacting layers have close optical transitions. In this case, major changes of the electronic structure can be observed and result in strong modifications of the optical absorption spectrum. In fact, energy shifts of “mirror” optical transitions, *i.e.* the transitions between mirror spikes of the density of states (DOS) of the DWNT (it can be recalled that in SWNTs mirror transitions are the only ones optically allowed for incident light polarization parallel to the nanotube main axis according to the selection rules) and, more strikingly, the appearance of strong absorption due to “cross-band” optical transitions (*i.e.*, between non-mirror spikes of the DOS). The presence of a cross transition is associated to the concomitant vanishing of absorption of mirror transitions [19];
- (ii) Significant mixing of the electronic states can be expected even for a relatively large difference of the transition energies of the non-interacting layers, resulting in absorption peaks of the cross transitions comparable to those of the mirror ones [19]. In this case, the model states

that a cross transition arises when spikes of the DOS have non-negligible contribution from both layers which can be interpreted as a significant mixing of their electronic states [19].

Clearly, the latter approach [19] is very appropriate for understanding the experimental optical spectra of any DWNTs regardless of their structure.

In the present work, the optical transitions of two index-identified individual DWNTs have been studied in detail by combining spatial modulation spectroscopy (SMS), resonant Raman scattering (RRS) and electron diffraction (ED), see Table 1. Although both DWNTs are expected to be weakly interacting according to Koshino's geometrical criteria, shifts (vs. SWNTs) of the optical transitions as large as 190 meV are evidenced and a new optical transition absent in the constituting SWNTs is observed. The experimental results are explained in the framework of calculations developed recently [19]. In particular, the new transition is attributed to a cross transition and its impact on the resonant behavior of the RBLM and G-modes is addressed experimentally.

2. Experimental methods

The experimental data recorded on carbon nanotubes, including those derived from optical absorption, Raman spectroscopy, photoluminescence, and Rayleigh scattering, drastically depend on the purity and environmental interactions in the carbon nanotube samples under investigation [41,45]. So, performing experiments on individual environment-free DWNTs is the most direct and unambiguous route to measure their intrinsic properties. In this aim ultra-long individual DWNTs were grown by the catalytic chemical vapor deposition (CCVD) method directly across home-made slits fabricated by wet-etching of a SiO₂/Si substrates [46].

Direct measurements of the absolute absorption cross-section spectra of freely suspended DWNTs were carried out via spatial modulation spectroscopy technique

[41,44,47,48]. This technique modulates the position of a single nanotube located under a tightly focused polarized laser beam and synchronously detects the induced modulation of the transmitted or reflected light power. Using a combination of different laser systems, a femtosecond Ti:Sapphire laser either pumping an optical parametric amplifier or generating second harmonics in a non-linear crystal, we measured the nanotubes absorption response over a large spectral range in the visible and near-infrared (390-950 nm or 1.3-3.2 eV) (for details about the experimental procedure see Ref. [48]).

The resonant Raman scattering measurements were performed on a home-made micro-Raman set-up fitted with an iHR550 spectrometer (Horiba JY), equipped with a LN₂-cooled Si CCD detector, using a wide variety of excitation wavelengths by using DPSS Laser Diodes, Ar⁺, Kr⁺, He-Ne lasers and continuous Ti:sapphire and dye lasers. The scattered light was collected through a 100X objective (NA = 0.95) using a backscattering configuration. In all the measurements, both incident and scattered light polarizations are along the nanotube axis. In order to avoid heating effects, the laser power impinging the sample was kept ~100 μW. Raman spectroscopy gives unique information on the features of the radial breathing-like modes (RBLMs) and G-modes in DWNTs; especially the REP of each mode gives information about its main origin: inner or outer tubes vibrations, and permits to evidence and to quantify the coupling between the layers [4,6,10,15,16,49].

High-resolution transmission electron microscope (HRTEM) images and electron diffraction patterns were recorded in an aberration corrected FEI Titan microscope operating at 80 kV and within short acquisition times (less than 5s for ED) to reduce damage induced by electron diffraction [50-52]. Comparison between simulated and experimental ED patterns allow for unambiguous identification of the chiral of nanotubes, (see Fig. S1).

All spatial modulation spectroscopy, resonant Raman scattering, and electron diffraction measurements were performed on the same suspended DWNTs, therefore providing

a unique combination of methods to investigate the optical, electronic, and vibrational properties of individual index-identified DWNTs.

3. Theoretical background

Most of the DWNTs, including the ones studied here, consist of layers of incommensurate periodicity, which rules out the direct use of band-structure computer codes for periodic or finite-size systems. The periodicity of the layers can still be used by considering the interlayer interaction as a perturbation, which allows for estimation of the shift of the optical transitions [17,18] but not for the prediction of additional transitions. The latter problem has been tackled successfully by the application of the recursion method [53] with the NTB model [54] in a recent study [19], and this computational approach is adopted here. The NTB model utilizes parameters for the Hamiltonian and the overlap matrix elements between s, px, py, and pz atomic orbitals of carbon, derived in ab-initio studies for the intralayer interactions [55] and the interlayer interactions [56]. The recursion method is implemented here to calculate the electronic density of states (DOS) and absorption coefficient of the DWNTs. In the former case, a 200 nm long piece of a DWNT with over 300,000 atomic orbitals, as well as 5,000 recursion iterations, are used for obtaining the optical transitions with an accuracy of 0.01 eV, comparable to the experimental error. In the latter case, a smaller piece of a DWNT of the length of 40 nm with over 60,000 orbitals, as well as 1,000 recursion iterations, are found sufficient for the prediction of new optical transitions. Similar calculations are performed for the separate layers of the DWNTs in order to derive the DOS and absorption coefficient for non-interacting layers. The comparison of the DOS for interacting and non-interacting layers yields the shift of the optical transitions, as well as the energy of the additional optical transitions, identified from the

corresponding spectra of the absorption coefficient (for details about the computational approach, see Ref. [19])

4. Results and discussion

In this work, we are mainly interested in evidence of the consequence of the interlayer interaction on the absorption. In this aim, we focus on the comparison between experimental and calculated absorption spectra of two specific DWNTs: the (16,12)@(27,10) and the (10,9)@(18,11). **Table 1** summarizes the structural information for these two DWNTs and **Figure S1** displays their electronic diffraction patterns. On the other hand, in relation to the absorption results, the analysis of the REPs of the RBLMs and G-modes permits addressing the impact of the interlayer coupling on the Raman intensities.

4.1 Absorption spectrum of (16,12)@(27,10) DWNT

The experimental absolute absorption spectrum of (16,12)@(27,10) DWNT measured in the 1.35-3 eV energy range for incident light polarized along the nanotube axis is displayed in **Figure 1a** (black dots). The experimental spectrum is composed of two main distinct features as identified previously in the absorption spectra of SWNTs [41], namely: well-defined resonant absorption peaks and a non-resonant quasi-constant absorption background. Each absorption peak in **Fig. 1a** is well reproduced by a Voigt profile being the convolution of an excitonic line, assumed to exhibit a Lorentzian shape, and the Gaussian spectral profile of the incident laser beam (grey line in **Fig. 1a**). In addition to these peaks, side-features are present in the spectrum (vertical arrows in **Fig. 1a**) and assigned as phonon side-bands (see Ref. [41] and references therein). The result of the fit captures the main absorption features except around 1.9-2.0 eV. However, according to Raman excitation profiles (see ref. [49] and **Fig. S2**), the

small feature around 1.98 eV is not associated to an optical transition and its origin remains an open question. Nevertheless, the overall good fit of the experimental data using the method detailed in Ref. [41] demonstrates the excitonic nature of absorption transitions of this DWNT. Six well-defined resonant peaks are observed at 1.44, 1.67, 1.81, 2.15, 2.44, and 2.76 eV. Their absolute absorption cross-section ($C_{\text{abs}}^{E_{ii}}$) were evaluated as 0.62, 0.51, 0.31, 0.15, 0.49, and 0.19 nm²/nm respectively (Table 2). The absorption cross-section of the absorption background ($C_{\text{abs}}^{\text{nr}}$) was evaluated at 0.15 nm²/nm (maximum deviations on the absorption measurements are ± 0.025 nm²/nm) (for details about the evaluation of the absorption cross-section, see Ref. [41]). The total absorption is defined as: $C_{\text{abs}} = C_{\text{abs}}^{E_{ii}} + C_{\text{abs}}^{\text{nr}}$, expressed as an absorption cross-section per unit of length of the nanotube ($C_{\text{abs,L}}$) or in units of cm² per carbon atom: $C_{\text{abs,C}} = C_{\text{abs,L}} a_{\text{C}}^2 (d_{\text{in}} + d_{\text{out}})$, where a_{C} is the radius of the equivalent surface occupied by a carbon atom in the crystalline lattice.

The Raman spectra of the (16,12)@(27,10) DWNT were recorded at excitation energies corresponding or close to the energies of the absorption peaks (Fig. 1c and 1d). All the Raman spectra excited at these energies clearly show radial breathing-like modes (RBLMs) and G-modes. The collective in-phase and out-of-phase RBLMs are observed respectively at 109 cm⁻¹ and 142 cm⁻¹ in good agreement with the predictions (110 cm⁻¹ and 141 cm⁻¹) of the mechanically coupled oscillator model [6] taking into account the environmental effects on the outer tube [4,52]. The G-modes present a narrow and symmetric line shape in agreement with the semiconducting character of both inner and outer tubes [57]. As stated in our recent work regarding the dependence of G-modes of DWNTs as a function of their atomic structure [10,12,15], the highest-frequency peak at ~ 1589 cm⁻¹ is assigned to the overlap of longitudinal optical G-mode of the outer (LO_{out}) and inner (LO_{in}) nanotubes; the two others peaks located at 1577 cm⁻¹ and 1568 cm⁻¹ are assigned to the transverse optical (TO) G-modes of the outer (TO_{out}) and inner (TO_{in}) tubes, respectively.

The excitation energy dependence of the Raman-active modes (RBLMs and G-modes) and the absorption broadband spectrum offer a unique combination of techniques allowing the unambiguous identification of each absorption transition. In the following, we designate each excitonic mirror transition of a DWNT by S_{ii}^{in} (S_{ii}^{out}) when this one mainly originates from the constituting semiconducting inner (outer) SWNT. By combining the experimental absorption and Raman spectra of the (16,12)@(27,10) DWNT, we propose that the peaks at 1.44, 1.67 and 2.44 eV originate from optical transitions of the outer tube because strong intensities of the in-phase RBLM and TO_{out} mode are observed at these energies. On the basis of optical transition energies measured and/or calculated on SWNTs [33,54], the energy transitions at 1.44 and 1.67 eV are identified as originating from the S_{33}^{out} and S_{44}^{out} , transition respectively, and the absorption at 2.44 eV encompasses both the S_{55}^{out} and S_{66}^{out} transitions (it can be emphasized that the unusual strong intensity of the TO_{out} mode in the Raman spectrum excited at 2.44 eV is ascribed to constructive quantum interferences [49]). The peaks at 1.81, 2.15, and 2.76 eV are associated with optical transitions of the inner tube since the out-of-phase RBLM dominates the Raman spectra recorded at these energies (Fig.1c) and, on the other hand, the TO_{in} mode is observed in the same spectra (Fig. 1d). Consequently, these transitions are identified as originating from the S_{33}^{in} , S_{44}^{in} and S_{55}^{in} transitions, respectively (Table 2). The energies of each absorption peak, their assignment and the experimental shifts of the different transitions with respect to the measured resonances in isolated SWNTs of the same chiral indices [33] are given in Table 2.

Figure 2a shows the calculated DOS of the (16,12)@(27,10) DWNT (black curve) in comparison with the DOS of the non-interacting (16,12) (blue curve) and (27,10) (red curve) layers. Figure 2b shows the contributions of the inner layer (blue line) and outer layer (red line) at the DOS of the (16,12)@(27,10) DWNT (black line). Clearly, the electronic structure of

DWNT is strongly perturbed by the interlayer interaction, which is seen as additional spikes in the DOS mainly for high energies (black curve in Fig. 2b).

The results of the calculation of the absorption coefficient of the (16,12)@(27,10) DWNT (red curve) are shown in Fig. 1b and Fig. S3 (Fig. S3 shows the results of the calculation in an extended energy range). On the same figures the calculation of the absorption coefficient for non-interacting (16,12) and (27,10) SWNTs ((16,12)+(27,10), blue dotted curve in Fig. 1b and Fig. S3) is shown and the assignment of each absorption peak is given. The number of peaks in (16,12)@(27,10) DWNT absorption spectrum is the same as in the calculated absorption coefficient of the inner and outer layers ((16,12)+(27,10), blue dotted curve in Fig. 1b and Fig. S3). In other words, no new transitions are predicted in (16,12)@(27,10) DWNT. Therefore, although the calculated DOS of DWNT looks complicated, the calculations of the absorption coefficient predict that the absorption is not perturbed below 1.3 eV (Fig.S3), and the absorption peaks are slightly changed and shifted above 1.3 eV (Fig.1b and Fig. S3).

Comparison between the experimental and calculated absorption coefficients is performed on Figure 1a and 1b. It must be emphasized that the optical transitions calculated in the 0.93-2.63 eV range correspond to the optical transitions measured in the 1.3-3 eV range. Indeed, calculations do not take into account the many-body effects related to the excitonic character of the transitions neither the electronic screening between the layers in DWNT. These two contributions explains the energy shifts between the experimental and calculated transitions. An average shift between the experimental and calculated transitions is estimated at about 370 meV. This 370 meV shift is in good agreement with the expected one resulting from the sum of a ≈ 430 meV blue shift due to many-body effects [16,52,58] and a ≈ 55 meV redshift related to dielectric screening [5,9] not included in the model. The excitonic nature of the transition vs. the single-particle approximation used for the calculations explain the different lineshape of the peaks which is symmetric in the experimental spectrum and asymmetric in the

theoretical one. Nevertheless, the calculations reasonably reproduce the general profile of the experimental absorption, especially they predict a significantly weaker intensity of the $S_{44,in}$ transition with respect to the intensities of the other transitions. Calculations also permit precisising the physical origin of each measured absorption peak (Fig. 1a). Although the electronic structure of the DWNT looks complicated due to the interlayer interaction, the contributions of the inner and outer layers of the DWNT reported in Fig. 2b show that the optical resonances originate from transitions between mirror spikes of the DOS with a one-to-one correspondence with the transitions of the non-interacting layers. No new cross-transition appears, and the assignment of the optical transitions as referred to the non-interacting layers agrees with the Raman conclusions.

In order to overcome the problem of the shift between the experimental and calculated transitions energies, we compare in Table 2 the experimental/calculated energy shifts of the DWNT optical transitions with respect to their experimental/calculated energies in the corresponding individual SWNTs. Doing so, we have access to a direct comparison between experiment and calculations of the energy differences between the DWNT and SWNTs transitions (see Table S1 for the list of transitions energies of the (16,12)@(27,10) DWNT and (16,12) and (27,10) SWNTs). Calculations predict a large redshift for the S_{44}^{in} transition (-130 meV), a significant redshift for the S_{55}^{in} (-80 meV), smaller redshifts for the $S_{55}^{out} + S_{66}^{out}$ (-50 meV) and S_{33}^{in} (-50 meV) transitions, and slight redshifts for the S_{44}^{out} (-20 meV) and S_{33}^{out} (-10 meV) transitions. On average, the calculated shifts differ from the experimental ones by -50 meV (+/-20 meV) and -30 meV (+/-35 meV) for the inner and outer layers, respectively. Given the 55 meV redshift related to dielectric screening [9] expected between the model and experiment, the data for the inner layer are in very good agreement and the deviations observed are within the experimental/calculation errors. Concerning the outer layer, the average shift differs significantly from the expected one, and the spreading of the data is beyond the

experimental/calculations errors. We interpret this discrepancy as the remaining environmental effect on the outer layer in our experiments, as evidenced by the up-shift of the in-phase RBLM (109 cm^{-1}) as compared to the value expected for an environment-free outer layer (97 cm^{-1}) [4, 52].

REPs of the RBLM and G-modes of this DWNT have been measured with laser excitations ranging from 1.3 to 2.7 eV [49]. As discussed in our previous paper [49], the observed intensity dependencies can be well understood using the common Raman intensity expression and taking into account interference effects. Looking at the data in more details, it can be noted that the relative intensity of the RBLMs changes from one transition to another. For example, the ratio of the maximum intensities of the in-phase vs. out-of-phase RBLM is ≈ 3 for the S_{33}^{out} transition and ≈ 10 for the S_{44}^{out} transition (see Fig. S2). This is at odds with the expectations that can be derived from the mechanically coupled oscillator model [6]. Indeed, within the framework of this model, this ratio should be constant for all S_{ii}^{out} (or S_{ii}^{in}) transitions when quantum interference effects can be neglected, *i.e.* when the separation in energy of successive transitions is large enough as for the S_{33}^{out} and S_{44}^{out} transitions considered here. This finding points out that the electronic coupling between the two layers has an impact on the Raman intensities though it is rather subtle in the case of this DWNT.

4.2 Absorption spectrum of (10,9)@(18,11) DWNT

The experimental absolute absorption spectrum of (10,9)@(18,11) DWNT was measured in the 1.3-3.05 eV energy range for incident light polarized along the nanotube axis (Figure 3a, dots (raw experimental data), black line is a guide for eyes). The absorption spectrum present six transitions located at 1.59, 1.89, 2.20, 2.42, 2.79 and 2.99 eV, with absorption cross-section 0.50, 0.12, 0.31, 0.35, 0.13 and 0.10 nm^2/nm respectively on top of the non-resonant absorption background of 0.23 nm^2/nm . On the same Figure 3a are displayed the

REP of the in-phase RBLM, located at 135 cm^{-1} (red curve in Fig. 3a) and that of the out-of-phase RBLM, located at 196 cm^{-1} (green curve in Fig. 3a) measured in the 1.2-2.0 eV excitation range. The REP of the in-phase RBLM exhibits resonances at 1.59 eV and 1.89 eV and that of the out-of-phase RBLM one at 1.26 eV and 1.59 eV. It can be emphasized that the REPs of the in-phase and out-of-phase RBLM are close in intensity around the resonance located at 1.59 eV. So, combining the absorption and REP data identifies seven transitions in the 1.2-3.05 eV range, namely 1.26, 1.59, 1.89, 2.20, 2.42, 2.79 and 2.99 eV.

The RBLM and G-modes regions of the Raman spectra of the (10,9)@(18,11) DWNT, recorded at excitation energies corresponding (or close) to the energies of the absorption peaks are shown in Fig. 3c-d. Depending on the excitation energy, two pairs of G-modes are clearly identified: $1592\text{-}1577 \text{ cm}^{-1}$ and $1586\text{-}1557 \text{ cm}^{-1}$. Regarding the dependence of G-modes of DWNTs as a function of their atomic structure [10,12,15], we can assign these pairs as $\text{LO}_{\text{out}}\text{-TO}_{\text{out}}$ pair and $\text{LO}_{\text{in}}\text{-TO}_{\text{in}}$ pair, respectively (Fig. 3d).

A single high-frequency mode assigned as the out-of-phase RBLM is observed in the RBLM range of the Raman spectra excited at 1.27 and 2.41 eV (Fig. 3c). On the other hand, the $\text{LO}_{\text{in}}\text{-TO}_{\text{in}}$ pair dominates the G-modes range of the Raman spectra excited at 1.44 and 2.54 eV corresponding to outgoing resonance conditions with the transitions at 1.26 and 2.42 eV for the inner tube G-modes (Fig. 3d). For an excitation at 2.41 eV, corresponding to incoming resonance, the $\text{LO}_{\text{in}}\text{-TO}_{\text{in}}$ pair is also observed but the $\text{LO}_{\text{out}}\text{-TO}_{\text{out}}$ pair is also present because of the outgoing resonance with the transition at 2.2 eV. Consequently, the 1.26 and 2.42 eV absorption peaks are associated with mirror transitions of the inner tubes, respectively the S_{22}^{in} and S_{33}^{in} transitions.

A single low-frequency mode assigned as the in-phase RBLM is observed in the spectra excited at 1.92 and 2.71 eV (Fig. 3c) and the $\text{LO}_{\text{out}}\text{-TO}_{\text{out}}$ pair is also observed at the same excitations (Fig. 3d) (note that, in the same spectra, the $\text{LO}_{\text{in}}\text{-TO}_{\text{in}}$ pair is present as well

due to outgoing resonances with the transitions at 1.59 and 2.42 eV). So the absorption peaks at 1.89 and 2.79 eV are assigned as S_{33}^{out} and S_{55}^{out} transitions.

Finally, the presence of the LO_{out}-TO_{out} pair in the spectra excited at 2.21 (incoming resonance) and 2.41 eV (outgoing resonance) (Fig. 3d) leads to assign the absorption peak at 2.20 eV as the S_{44}^{out} transition. It can be emphasized that no low-frequency RBLM is observed in the Raman spectrum excited at 2.21 eV. The vanishing of the in-phase RBLM at the 2.21 eV excitation is consistent with theoretical calculations [59], which predicts a low intensity for the RBM excited close of the S_{44} transition in the (18,11) SWNT.

To sum up, the analysis of excitation dependence of the Raman spectra allows the identification of five transitions in the 1.2-2.8 eV energy range (1.26, 1.89, 2.20, 2.42, 2.79 eV) which are associated to mirror transitions in DWNTs involving inner or outer layers. Additionally, the absorption peak at 2.99 eV can be tentatively attributed to the S_{44}^{in} transition. Clearly, the 1.59 eV absorption peak cannot be attributed to a corresponding mirror transition of the constituting SWNTs. Moreover, it exhibits a particular behavior since both RBLMs are observed with comparable intensities for excitation at this energy conversely to all other transitions where a single RBLM largely dominates the Raman response. This difference points out that another effect beyond mechanical coupling [6] is involved. In conclusion, the 1.59 eV absorption peak has to be associated with an additional transition not present for the constituting SWNTs. The energies of each absorption peak, their assignment and the experimental shifts of the different transitions with respect to the measured resonances in isolated SWNTs of the same chiral indices [33] are given in Table 3.

Figure 4a (black curve) shows the calculated DOS of the (10,9)@(18,11) DWNT in comparison with the DOS of the non-interacting (10,9) (blue line in Fig. 4a) and (18,11) (red line in Fig. 4a) layers. The horizontal arrows between the mirror spikes mark the optical transitions in the investigated experimental energy range for the non-interacting layers. In the

1.2-2.8 eV energy range, in agreement with the Raman conclusions, the optical resonances at 1.26, 1.89, 2.20, 2.42, 2.79 eV in DWNT originate from transitions between mirror spikes of the DOS with a one-to-one correspondence with the transitions of the non-interacting layers. Calculations predict the upshift of S_{33}^{out} and S_{55}^{out} transitions and the downshift of all other mirror transitions in the DWNT as compared to the constituting SWNTs. The directions of these shifts are in agreement with the experimental data (see [Table 3](#)).

[Figure 4b](#) shows the contributions of the (10,9) inner layer (blue line) and (18,11) outer layer (red line) to the DOS of the (10,9)@(18,11) DWNT (black line). It is clear that the electronic states of the two layers associated with transitions S_{22}^{in} and S_{33}^{out} strongly couple in this DWNT. As shown in [Figure 4a](#), this coupling produces shifts of the mirror spikes of these states in DWNT. More strikingly, it is seen that these spikes have contributions from the states of both layers leading to additional transitions, shown as S_{mix}^a and S_{mix}^b on [Figure 4b](#).

The results of the calculation of the absorption coefficient of the (10,9)@(18,11) DWNT are shown on [Fig. 3b](#) (red line) and [Fig. S4](#) ([Fig. S4](#) shows the results of the calculation in an extended energy range), and compared to the calculated absorption coefficient for non-interacting (10,9) and (18,11) SWNTs (blue dotted curve). This comparison allows the assignment of most absorption peaks in DWNT as originating from mirror transitions in non-interacting layers. This confirms unambiguously the presence of a new absorption band at around 1.3 eV (uncorrected theoretical value) in this DWNT (red arrow in [Fig.3b](#)). The coupling between the S_{22}^{in} and S_{33}^{out} transitions, already put in evidence from the DOS ([Fig.4b](#)), manifests itself in the absorption spectrum by a significant downshift of the S_{22}^{in} transition and a significant upshifts of the S_{33}^{out} transition. Given the relatively large difference between the the S_{22}^{in} and S_{33}^{out} energies, the electronic states mixing scenario corresponds to the second case reported in ref. [\[19\]](#) and summarized in the introduction part (ii). The peaks of the other transitions seem to be slightly affected by the interlayer interactions.

Comparison between the experimental and calculated absorption coefficients is performed on [Figure 3a](#) and [3b](#). The optical transitions calculated in the 0.9-2.8 eV range correspond to the optical transitions measured in the 1.24-3.14 eV range. As previously, the shift between the experimental and calculated transitions is due to the lack of consideration of the many-body effects and dielectric screening in the calculations. For this DWNT, we have estimated an average shift between the experimental and calculated transitions close of 340 meV (this shift puts in coincidence the central part of experimental and calculated absorption spectra). By taking into account this shift, the profile of the calculated absorption coefficient (red line in [Fig.3b](#),) exhibits a relatively good agreement with the experimental one (black line in [Fig.3a](#)). Except for the position of the S_{22}^{in} transition, and to a lesser extent that of the S_{33}^{in} transition, which are upshifted in the calculations, the positions of the calculated absorption peaks are close to the experimental ones. Finally, the model predicts a weakening of the coupled S_{22}^{in} and S_{33}^{out} with regards to the intensity of the S_{44}^{out} and S_{33}^{in} transitions as experimentally observed for the S_{33}^{out} (the S_{22}^{in} is out of the experimental absorption range).

A quantitative comparison between the calculated versus experimental energy shifts of the DWNT optical transitions with respect to their calculated/experimental energies in the corresponding individual SWNTs is presented in [Table 3](#) (see [Table S2](#) for the list of transitions energies of the (10,9)@(18,11) DWNT and (10,9) and (18,11) SWNTs). Large experimental redshifts are measured for the S_{22}^{in} (-135 meV) and S_{33}^{in} (-145 meV) transitions and a smaller one (-15 meV) is observed for the S_{44}^{in} transition. Calculated shifts are predicted at -80 meV, -70 meV and +10 meV respectively for the same transitions. By applying at the calculated shifts a 55 meV redshift, related to dielectric screening [\[9\]](#), the calculated and experimental shifts are in good agreement for the S_{22}^{in} , S_{33}^{in} and S_{44}^{in} transitions (the differences between experimental and calculated shifts are, respectively, 0, -20 and +30 meV what falls within the expected error). Experimental upshifts of the S_{33}^{out} (85 meV) and S_{55}^{out} (10 meV) transitions and a large

experimental redshift of the S_{44}^{out} (-90 meV) transition are measured. The corresponding calculated shifts are evaluated at 80, 10 and -10 meV, respectively (Table 3). Applying the rigid additional downshift due to the screening effect (~55 meV from Ref. [9]) leads to calculated shifts, which differ significantly from expected ones, especially for the S_{33}^{out} and S_{55}^{out} transitions. Striking, for the latter transitions, it seems that the downshift due to screening effect is totally compensated by an upshift possibly due to other interactions, including environmental effects.

It is worth highlighting that our combined experimental and theoretical approach leads to the unambiguous assignment of the experimental absorption peak at 1.59 eV as originating from transitions between non-mirror spikes of the DOS. It has to be reminded that additional transitions were previously observed in (12,11)@(17,16) DWNT [17]. The origin of this additional transitions was attributed to the strong interlayer coupling effect in the Moiré superlattice formed by two nearly armchair nanotubes following the so-called Koshino's criteria which predict the appearance of such transition (the so-called strong-coupling regime) [11]. For the (15,13)@(21,17) DWNT, the number of peaks in the Rayleigh spectrum measured in Ref. [17] matches well with the one expected for each individual constituent nanotubes what leads the authors of Ref. [17] to conclude that no additional transition is present in this DWNT. However, the theoretical analyses reported on Ref. [19] suggest that this conclusion should be revised putting forward that some of the observed transitions are new transitions (i.e. cross transitions), see Ref. [19] for more details. The theoretically predicted concomitant vanishing of some mirror transitions explains that the number of peaks in the Rayleigh spectrum remains unchanged. Nevertheless, this (15,13)@(21,17) DWNT is also expected to be in the strong coupling regime as defined in Ref. [11]. On the contrary, the (10,9)@(18,11) DWNT studied here would be classified as in a weak coupling regime. Thus, our work puts in evidence that the presence of additional non-mirror transitions in DWNT can be observed beyond Koshino's

criteria. In the (10,9)@(18,11) DWNT, a significant mixing of the electronic states for relatively large difference of the transition energies of the non-interacting layers leads to an additional cross transition comparable in intensity to those of the mirror transition [19].

Finally, the analysis of the REP of the RBLMs and G-modes reveals the specific nature of the cross transition (*i.e.* non-mirror transition) at 1.59 eV. As shown in Figure 3a (see also the maps in the Supplement Information, Figure S5), the in-phase and out-of-phase RBLMs show a close excitation dependence of their intensity around the S_{mix} transition.

More striking is the excitation dependence of the G-modes in the S_{mix} excitation range. Spectra excited at S_{mix} and $S_{mix}+E_{G-mode}$ are shown in Figure 5a (E_{G-mode} is the G-mode energy). The LO_{out}-TO_{out} pair (respectively LO_{in}-TO_{in} pair) dominates the spectrum at the S_{mix} (respectively $S_{mix}+E_{G-mode}$) excitation. It can be reminded that for excitation around the S_{mix} transition, the in-phase and out-of-phase RBLM appear in the same spectrum (see the spectrum excited at 1.61 eV in Figure 3c).

To complete our information, we have measured the excitation dependence of the intensity of each LO and TO G-mode in the 1.4-2 eV excitation range. The corresponding REPs are shown in Figure 5b (LO_{out} (red curve) and LO_{in} (blue curve)) and Figure 5c (TO_{out} (red curve) and TO_{in} (blue curve)). The REP of each mode is complex, with a well-identified primary maximum and the presence of secondary maxima and shoulders. These REPs differ significantly from the usual profile of the REPs of G-modes measured on SWNTs [35] and DWNTs [49] when these DWNTs do not show cross transitions. The more striking and important result is the significant difference between the REPs of each pair of G-modes. Especially the primary resonance occurs at different energies for the two pairs of G-modes, namely around S_{mix} (1.59 eV) for the LO_{out}-TO_{out} pair and around $S_{mix}+E_{G-mode}$ (1.79 eV) for LO_{in}-TO_{in} pair (Figure 5b and Figure 5c).

Our results clearly illustrate the strong sensitivity of the REP of the G-modes on the electronic interlayer coupling in DWNT. From a general point of view, these results point out Raman spectroscopy as a powerful tool to clearly identify the nature of the optical transitions in DWNTs and to distinguish between mirror and cross transitions in a more direct and error-proof way than optical absorption or Rayleigh scattering measurements. Further theoretical developments are required for getting a better understanding of these very interesting results.

5. Conclusion

By combining spatial modulation spectroscopy (SMS) and resonant Raman scattering (RRS) experiments on well-identified individual free-standing (suspended) double-walled carbon nanotubes (DWNTs) with the calculations of their optical absorption by using the recursion method with non-orthogonal tight-binding (NTB) basis functions [19], we unambiguously assign the nature, namely mirror transition or cross transition, of each optical transitions in DWNTs.

This combined approach also permits understanding the origin of the experimental upshift or downshift of mirror transitions in the DWNT as compared to the energies of the mirror transitions in the constituting SWNTs.

Our study states that the presence of cross transitions in DWNTs, beyond previously derived criteria [11], can be observed when a significant mixing of the electronic states of the transition energies of the non-interacting layers exists and can be predicted within the framework of a realistic microscopic model [19].

Finally, the RBLM relative intensity is shown to be sensitive to the mixing of the electronic states of the layers and not only to their mechanical coupling [5] nor quantum interferences between transitions [6]. The striking behavior of the REPs of the G-modes around the studied cross transition reveals the strong sensitivity of the G-modes intensity on the

electronic interlayer coupling in DWNTs. More generally, the relevance of Raman spectroscopy for studying the electronic and mechanical coupling at the nanoscale can be emphasized.

Acknowledgements

We acknowledge the Dr. T. X. Tinh for the synthesis of individual nanotubes. HNT, RP, AAZ, JLS and MP acknowledge financial support by the ANR GAMBIT project, grant ANR-13-BS10-0014 of the French Agence Nationale de la Recherche.

The TEM studies were performed in the Laboratorio de Microscopias Avanzadas (LMA), Universidad de Zaragoza (Spain). R.A. acknowledges support from Spanish MICINN (PID2019-104739GB-100/AEI/10.13039/501100011033), Government of Aragon (projects DGA E13-20R (FEDER, EU)) and from EU H2020 “ESTEEM3” (Grant number 823717).

VNP acknowledges financial support for NTB calculations from the National Science Fund of Bulgaria under grant KP-06-N38/10 from 06.12.2019.

References

- [1] Mogeraa, U.; Kulkarniab, G. U. A new twist in graphene research: Twisted graphene. *Carbon* **2020**, *156*, 470-487.
- [2] Kim, Y. A.; Yang, K.-S.; Muramatsu, H.; Hayashi, T.; Endo, M.; Terrones, M.; Dresselhaus, M. S. Double-Walled Carbon Nanotubes: Synthesis, Structural Characterization, and Application. *Carbon Lett.* **2014**, *15*, 77–88.
- [3] Zhao, S.; Kitaura, R.; Moon, P.; Koshino, M.; Wang, F. Interlayer Interactions in 1D Van Der Waals Moiré Superlattices. *Adv. Sci.* **2022**, *9*, 2103460.
- [4] Levshov, D.; Than, T. X.; Arenal, R.; Popov, V. N.; Parret, R.; Paillet, M.; Jourdain, V.; Zahab, A. A.; Michel, T.; Yuzyuk, Y. I.; et al. Experimental Evidence of a Mechanical Coupling between Layers in an Individual Double-Walled Carbon Nanotube. *Nano Lett.* **2011**, *11*, 4800–4804.
- [5] Tomio, Y.; Suzuura, H.; Ando, T. Interwall Screening and Excitons in Double-Wall Carbon Nanotubes. *Phys. Rev. B: Condens. Matter Mater. Phys.* **2012**, *85* (8), 085411.
- [6] Liu, K.; Hong, X.; Wu, M.; Xiao, F.; Wang, W.; Bai, X.; Ager, J. W.; Aloni, S.; Zettl, A.; Wang, E.; et al. Quantum-Coupled Radial-Breathing Oscillations in Double-Walled Carbon Nanotubes. *Nat. Commun.* **2013**, *4*, 1375.
- [7] Hirschmann, T. C.; Araujo, P. T.; Muramatsu, H.; Rodriguez-Nieva, J. F.; Seifert, M.; Nielsch, K.; Kim, Y. A.; Dresselhaus, M. S. Role of Intertube Interactions in Double- and Triple-Walled Carbon Nanotubes. *ACS Nano* **2014**, *8*, 1330–1341.
- [8] Zhao, S.; Kitagawa, T.; Miyauchi, Y.; Matsuda, K.; Shinohara, H.; Kitaura, R. Rayleigh Scattering Studies on Inter-Layer Interactions in Structure-Defined Individual Double-Wall Carbon Nanotubes. *Nano Res.* **2014**, *7*, 1548–1555.
- [9] Liu, K.; Jin, C.; Hong, X.; Kim, J.; Zettl, A.; Wang, E.; Wang, F. Van Der Waals-Coupled Electronic States in Incommensurate Double-Walled Carbon Nanotubes. *Nat. Phys.* **2014**, *10*, 737–742.
- [10] Levshov, D. I.; Michel, T.; Arenal, R.; Tran, H. N.; Than, T. X.; Paillet, M.; Yuzyuk, Y. I.; Sauvajol, J.-L. Interlayer Dependence of G-Modes in Semiconducting Double-Walled Carbon Nanotubes. *J. Phys. Chem. C* **2015**, *119*, 23196–23202.

- [11] Koshino, M.; Moon, P.; Son, Y.-W. Incommensurate Double-Walled Carbon Nanotubes as One-Dimensional Moiré Crystals. *Phys. Rev. B* **2015**, 91, 035405.
- [12] Levshov, D. I.; Tran, H. N.; Michel, T.; Cao, T. T.; Nguyen, V. C.; Arenal, R.; Popov, V. N.; Sauvajol, J.-L.; Zahab, A.-A.; Paillet, M. Interlayer Interaction Effects on the G Modes in Double-Walled Carbon Nanotubes With Different Electronic Configurations. *Phys. Status Solidi* **2017**, 254 (11), 1700251.
- [13] Ghedjatti, A.; Magnin, Y.; Fossard, F.; Wang, G.; Amara, G.; Flahaut, E.; Lauret, J.-S.; Loiseau, A. Structural Properties of Double-Walled Carbon Nanotubes Driven by Mechanical Interlayer Coupling. *ACS Nano* **2017**, 11(5), 4840–4847.
- [14] Levshov, D. I.; Parret, R.; Tran, H.-N.; Michel, T.; Cao, T. T.; Nguyen, V. C.; Arenal, R.; Popov, V.N.; Rochal, S.B.; Sauvajol, J.-L.; Zahab, A.-A.; Paillet, M. Photoluminescence from an individual double-walled carbon nanotube. *Phys. Rev. B* **2017**, 96 (19), 195410.
- [15] Popov, V. N.; Levshov, D. I.; Sauvajol, J.-L.; Paillet, M. Computational Study of the Shift of the G Band of Double-Walled Carbon Nanotubes Due to Interlayer Interactions. *Phys. Rev. B* **2018**, 97 (16), 165417.
- [16] Michel, T.; Levshov, D.; Zahab, A.-A.; Sauvajol, J.-L.; Paillet, M. Probing the Intrinsic Vibrational and Optical Properties of Individual Chirality-Identified Carbon Nanotubes by Raman Spectroscopy. *Handbook of Carbon Nanomaterials* **2019** Vol. 10, Eds. B. Weisman and J. Kono, World scientific Publishing.
- [17] Zhao, S.; Moon, P.; Miyauchi, Y.; Nishihara, T.; Matsuda, K.; Koshino, M.; Kitaura, R. Observation of Drastic Electronic-Structure Change in a One-Dimensional Moiré Superlattice. *Phys. Rev. Lett.* **2020**, 124, 106101.
- [18] Chalin, D. V.; Rochal, S. B. Band structure and inter-tube optical transitions in double-walled carbon nanotubes. *Phys. Rev. B* **2020** 102, 115426.
- [19] Popov, V. N. Theoretical evidence of a significant modification of the electronic structure of double-walled carbon nanotubes due to the interlayer interaction. *Carbon* **2020** 170, 30-36.
- [20] Gordeev, G.; Wasserroth, S.; Li, H.; Flavel, B.; Reich, S. Moiré-Induced Vibrational Coupling in Double-Walled Carbon Nanotubes. *Nano Lett.* **2021**, 21(16), 6732–6739.

- [21] Aguiar, A. L.; Barros, E. B.; Capaz, R. B.; Souza Filho, A. G.; Freire, P. T. C.; Mendes Filho, J.; Machon, D.; Caillier, Ch.; Kim, Y. A.; Muramatsu, H.; Endo, M.; San-Miguel, A. Pressure-Induced Collapse in Double-Walled Carbon Nanotubes: Chemical and Mechanical Screening Effects. *J. Phys. Chem. C* **2011**, 115(13), 5378–5384.
- [22] Shen, C.; Brozena, A. H.; Wang, Y. Double-Walled Carbon Nanotubes: Challenges and Opportunities. *Nanoscale* **2011**, 3, 503–518.
- [23] Jariwala, D.; Sangwan, V. K.; Lauhon, L. J.; Marks, T. J.; Hersam, M. C. Carbon Nanomaterials for Electronics, Optoelectronics, Photovoltaics, and Sensing. *Chem. Soc. Rev.* **2013**, 42, 2824–2860.
- [24] Moore, K. E.; Tune, D. D.; Flavel, B. S. Double-Walled Carbon Nanotube Processing. *Adv. Mater.* **2015**, 27, 3105–3137.
- [25] Volder, M. F. L. D.; Tawfick, S. H.; Baughman, R. H.; Hart, A. J. Carbon Nanotubes: Present and Future Commercial Applications. *Science* **2013**, 339, 535–539.
- [26] Qian, L.; Xie, Y.; Zou, M.; Zhang, J. Building a Bridge for Carbon Nanotubes from Nanoscale Structure to Macroscopic Application. *J. Am. Chem. Soc.* **2021**, 143 (45), 18805–18819.
- [27] Tsyboulski, D. A.; Hou, Y.; Fakhri, N.; Ghosh, S.; Zhang, R.; Bachilo, S. M.; Pasquali, M.; Chen, L.; Liu, J.; Weisman, R. B. Do Inner Shells of Double-Walled Carbon Nanotubes Fluoresce? *Nano Lett.* **2009**, 9 (9), 3282–3289.
- [28] Miyata, Y.; Suzuki, M.; Fujihara, M.; Asada, Y.; Kitaura, R.; Shinohara, H. Solution-Phase Extraction of Ultrathin Inner Shells from Double-Wall Carbon Nanotubes. *ACS Nano* **2010**, 4 (10), 5807–5812.
- [29] Erkens, M.; Cambré, S.; Flahaut, E.; Fossard, F.; Loiseau, A.; Wenseleers, W. Ultrasonication-induced extraction of inner shells from double-wall carbon nanotubes characterized via in situ spectroscopy after density gradient ultracentrifugation. *Carbon* **2021**, 185 (15), 113-125.
- [30] Sfeir, M. Y.; Wang, F.; Huang, L.; Chuang, C.-C.; Hone, J.; O'brien, S. P.; Heinz, T. F.; Brus, L. E. Probing Electronic Transitions in Individual Carbon Nanotubes by Rayleigh Scattering. *Science* **2004**, 306, 1540–1543.

- [31] Sfeir, M. Y.; Beetz, T.; Wang, F.; Huang, L.; Huang, X. M. H.; Huang, M.; Hone, J.; O'Brien, S.; Misewich, J. A.; Heinz, T. F.; et al. Optical Spectroscopy of Individual Single-Walled Carbon Nanotubes of Defined Chiral Structure. *Science* **2006**, 312, 554–556.
- [32] Berciaud, S.; Voisin, C.; Yan, H.; Chandra, B.; Caldwell, R.; Shan, Y.; Brus, L. E.; Hone, J.; Heinz, T. F. Excitons and High-Order Optical Transitions in Individual Carbon Nanotubes: A Rayleigh Scattering Spectroscopy Study. *Phys. Rev. B* **2010**, 81, 041414(R).
- [33] Liu, K.; Deslippe, J.; Xiao, F.; Capaz, R. B.; Hong, X.; Aloni, S.; Zettl, A.; Wang, W.; Bai, X.; Louie, S. G.; Wang, E.; Wang, F. An atlas of carbon nanotube optical transitions. *Nat. Nanotechnol.* **2012**, 7, 325–329.
- [34] Yao, F.; Yu, W.; Liu, C.; Su, Y.; You, Y.; Ma, H.; Qiao, R.; Wu, C.; Ma, C.; Gao, P.; Xiao, F.; Zhao, J.; Bai, X.; Sun, Z.; Maruyama, S.; Wang, F.; Zhang, J.; Liu, K. Complete Structural Characterization of Single Carbon Nanotubes by Rayleigh Scattering Circular Dichroism. *Nat. Nanotechnol.* **2021**, 16 (10), 1073–1078.
- [35] Tran, H. N.; Blancon, J.-C.; Huntzinger, J.-R.; Arenal, R.; Popov, V. N.; Zahab, A. A.; Ayari, A.; San-Miguel, A.; Vallée, F.; Del Fatti, N.; Sauvajol, J.-L.; Paillet, M. Excitonic optical transitions characterized by Raman excitation profiles in single-walled carbon nanotubes *Phys. Rev. B* **2016**, 94, 075430.
- [36] Lefebvre, J.; Finnie, P. Polarized Photoluminescence Excitation Spectroscopy of Single-Walled Carbon Nanotubes. *Phys. Rev. Lett.* **2007**, 98, 167406.
- [37] Berciaud, S.; Cognet, L.; Lounis, B. Luminescence Decay and the Absorption Cross Section of Individual Single-Walled Carbon Nanotubes. *Phys. Rev. Lett.* **2008**, 101, 077402.
- [38] Berciaud, S.; Cognet, L.; Poulin, P.; Weisman, R. B.; Lounis, B. Absorption Spectroscopy of Individual Single-Walled Carbon Nanotubes. *Nano Lett.* **2007**, 7, 1203–1207.
- [39] Lefebvre, J.; Finnie, P. Polarized Light Microscopy and Spectroscopy of Individual Single-Walled Carbon Nanotubes. *Nano Res.* **2011**, 4, 788–794.
- [40] Oudjedi, L.; Parra-Vasquez, A. N. G.; Godin, A. G.; Cognet, L.; Lounis, B. Metrological Investigation of the (6,5) Carbon Nanotube Absorption Cross Section. *J. Phys. Chem. Lett.* **2013**, 4, 1460–1464.

- [41] Blancon, J.-C.; Paillet, M.; Tran, H. N.; Than, X. T.; Guebrou, S. A.; Ayari, A.; Miguel, A. S.; Phan, N.-M.; Zahab, A.-A.; Sauvajol, J.-L.; Del Fatti, N.; Vallée, F. Direct Measurement of the Absolute Absorption Spectrum of Individual Semiconducting Single-Wall Carbon Nanotubes. *Nat. Commun.* **2013**, 4, 2542.
- [42] Liu, K.; Hong, X.; Choi, S.; Jin, C.; Capaz, R. B.; Kim, J.; Wang, W.; Bai, X.; Louie, S. G.; Wang, E.; Wang F. Systematic Determination of Absolute Absorption Cross-Section of Individual Carbon Nanotubes. *Proc. Natl. Acad. Sci.* **2014**, 111, 7564–7569.
- [43] Yao, F.; Liu, C.; Chen, C.; Zhang, S.; Zhao, Q.; Xiao, F.; Wu, M.; Li, J.; Gao, P.; Zhao, J.; Bai, X.; Maruyama, S.; Yu, D.; Wang, E.; Sun, Z.; Zhang, J.; Wang, F.; Liu, K. Measurement of Complex Optical Susceptibility for Individual Carbon Nanotubes by Elliptically Polarized Light Excitation. *Nat. Commun.* **2018**, 9 (1), 3387.
- [44] Crut, A.; Maioli, P.; Del Fattia, N.; Vallée, F. Optical absorption and scattering spectroscopies of single nano-objects. *Chem. Soc. Rev.*, **2014**, 43, 3921-3956.
- [45] Hertel, T.; Walkup, R.E.; Avouris, P. Deformation of carbon nanotubes by surface van der Waals forces. *Phys. Rev. B* **1998**, 58, 13870.
- [46] Tinh, T. X.; Van Chuc, N.; Jourdain, V.; Paillet, M.; Kim, D.-Y.; Sauvajol, J.-L.; Tam, N. T. T.; Minh, P. N. Synthesis of Individual Ultra-Long Carbon Nanotubes and Transfer to Other Substrates. *J. Exp. Nanosci.* **2011**, 6, 547–556.
- [47] Arbouet, A.; Christofilos, D.; Del Fatti, N.; Vallée, F.; Huntzinger, J.-R.; Arnaud, L.; Billaud, P.; Broyer, M. Direct Measurement of the Single-Metal-Cluster Optical Absorption. *Phys. Rev. Lett.* **2004**, 93, 127401.
- [48] Christofilos, D.; Blancon, J.-C.; Arvanitidis, J.; Miguel, A. S.; Ayari, A.; Del Fatti, N.; Vallée, F. Optical Imaging and Absolute Absorption Cross Section Measurement of Individual Nano-Objects on Opaque Substrates: Single-Wall Carbon Nanotubes on Silicon. *J. Phys. Chem. Lett.* **2012**, 3, 1176–1181.
- [49] Tran, H. N.; Blancon, J. C.; Arenal, R.; Parret, R.; Zahab, A. A.; Ayari, A.; Vallée, F.; Del Fatti, N.; Sauvajol, J. L. ; Paillet, M. Quantum interference effects on the intensity of the G modes in double-walled carbon nanotubes. *Phys. Rev. B* **2017**, 95, 205411.

- [50] Arenal, R.; Kociak, M.; Loiseau, A.; Miller, D.-J. Determination of Chiral Indices of Individual Single- and Double-Walled Boron Nitride Nanotubes by Electron Diffraction. *Appl. Phys. Lett.* **2006**, *89*, 073104.
- [51] Arenal, R.; Löthman, P.; Picher, M.; Than, T.; Paillet, M.; Jourdain, V. Direct Evidence of Atomic Structure Conservation Along Ultra-Long Carbon Nanotubes. *J. Phys. Chem. C* **2012**, *116*, 14103–14107.
- [52] Levshov, D. I.; Tran, H. N.; Paillet, M.; Arenal, R.; Than, X. T.; Zahab, A. A.; Yuzyuk, Y. I.; Sauvajol, J.-L.; Michel, T. Accurate determination of the chiral indices of individual carbon nanotubes by combining electron diffraction and Resonant Raman spectroscopy. *Carbon* **2017** *114*, 141.
- [53] Haydock R.; Heine V.; Kelly M. J. Electronic structure based on the local atomic environment for tight-binding bands: II. *J. Phys. C: Solid State Phys.* **1975**, *8*, 2591.
- [54] Popov, V. N. Curvature Effects on the Structural, Electronic and Optical Properties of Isolated Single-Walled Carbon Nanotubes within a Symmetry-Adapted Non-Orthogonal Tight-Binding Model. *New J. Phys.* **2004**, *6*, 17–17.
- [55] Porezag D.; Frauenheim Th.; Köhler Th.; Seifert G.; Kaschner R. Construction of tight-binding-like potentials on the basis of density-functional theory: Application to carbon. *Phys. Rev. B* **1995**, *51*, 12947.
- [56] Popov V.N.; Van Alsenoy C. Low-frequency phonons of few-layer graphene within a tight-binding model. *Phys. Rev. B* **2014**, *90*, 245429.
- [57] Paillet, M.; Michel, T.; Meyer, J. C.; Popov, V. N.; Henrard, L.; Roth, S.; Sauvajol, J.-L. Raman Active Phonons of Identified Semiconducting Single-Walled Carbon Nanotubes. *Phys. Rev. Lett.* **2006**, *96*, 257401.
- [58] Michel, T.; Paillet, M.; Meyer, J. C.; Popov, V. N.; Henrard, L.; Sauvajol, J.-L. E33 and E44 Optical Transitions in Semiconducting Single-Walled Carbon Nanotubes: Electron Diffraction and Raman Experiment. *Phys. Rev. B* **2007**, *75*, 155432.
- [59] Popov, V.N.; Lambin, P. Resonant Raman intensity of the totally symmetric phonons of single-walled carbon nanotubes. *Phys. Rev. B*, **2006**, *73* (16), 165425.

	Indices	Type	diameter (nm)	Chiral angle (°)	$\Delta d/2$ (nm)
DWNT1	(16,12)@(27,10)	$S_I@S_{II}$	1.905@2.595	25.6@15.1	0.345
DWNT2	(10,9)@(18,11)	$S_I@S_I$	1.289@1.985	28.3@22.1	0.348

Table 1. Structural information for the DWNTs investigated in this work. Chiral indices were derived from electron diffraction measurements.

Optical transition	Exp. transition energy (eV)	DWNT vs. SWNTs transition energy shift (meV)		
		Exp.	Calc.	Exp. – Calc.
S_{33}^{out}	1.44	-70	-10	-60
S_{44}^{out}	1.67	-50	-20	-30
S_{33}^{in}	1.81	-75	-50	-25
S_{44}^{in}	2.15	-190	-130	-60
$S_{55}^{out} + S_{66}^{out}$	2.44	-45	-50	5
S_{55}^{in}	2.76	-135	-80	-55

Table 2. Optical transitions characteristics of the (16,12)@(27,10) DWNT (*DWNT 1*). The DWNT vs. SWNTs experimental energy shift is calculated by subtracting to the experimental transition energy of the DWNT, the corresponding SWNT one. This latter is determined by using the empirical formula of Ref. [33]. The DWNT vs. SWNTs calculated energy shift is the difference between the calculated transitions energies of the DWNT and the corresponding calculated transitions of the constituting SWNTs. The last column corresponds to the difference between experimental (column 4) and calculated (column 5) DWNT transitions energy shifts relative to corresponding SWNTs.

Optical transition	Exp. transition energy (eV)	DWNT vs. SWNTs transition energy shift (meV)		
		Exp.	Calc.	Exp. – Calc.
S_{22}^{in}	1.26*	-135	-80	-55
S_{mix}	1.59	/	/	/
S_{33}^{out}	1.89	85	80	5
S_{44}^{out}	2.2	-90	-10	-80
S_{33}^{in}	2.42	-145	-70	-75
S_{55}^{out}	2.79	10	10	0
S_{44}^{in}	2.99	-15	10	-25

Table 3. Optical transitions characteristics of the (10,9)@(18,11) DWNT (*DWNT 2*). The DWNT vs. SWNTs experimental energy shift is calculated by subtracting to the experimental transition energy of the DWNT, the corresponding SWNT one. This latter is determined by using the empirical formula of Ref. [33]. The DWNT vs. SWNTs calculated energy shift is the difference between the calculated transitions energies of the DWNT and the corresponding calculated transitions of the constituting SWNTs. The last column corresponds to the difference between experimental (column 4) and calculated (column 5) DWNT transitions energy shifts relative to corresponding SWNTs. *Determined using Raman RBLM excitation profile.

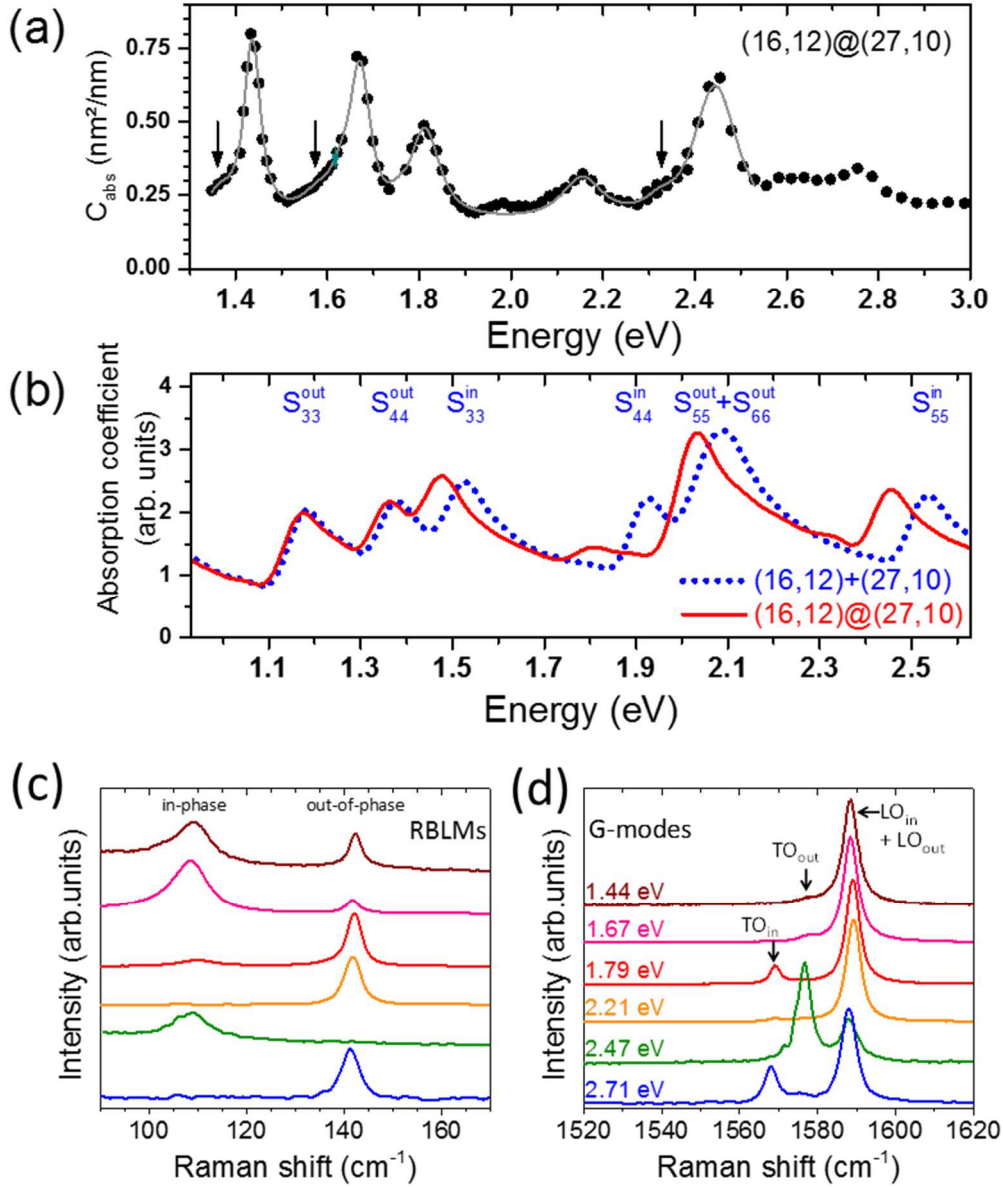


Figure 1: (a) Absolute absorption cross-section spectra of the (16,12)@(27,10) DWNT for incident light polarization parallel to the DWNT axis, black dots (experimental) and grey line (fit of the experimental data, see text). (b) The calculated absorption coefficient of the (16,12)@(27,10) DWNT (red line) in comparison with that for a DWNT without interlayer interaction (dotted blue line). The blue S_{ii}^{in} and S_{ii}^{out} labels indicate the optical transitions of the inner and outer layers, respectively. Note that the energy scale of panel (b) has an offset of -370 meV relative to panel (a) in order to facilitate the direct comparison between experiment and theory, see main text. (c) and (d) Raman spectra of the individual free-standing (16,12)@(27,10) DWNT recorded at different excitation energies as labeled on the left hand side of (d): (c) RBLMs and (d) G-modes.

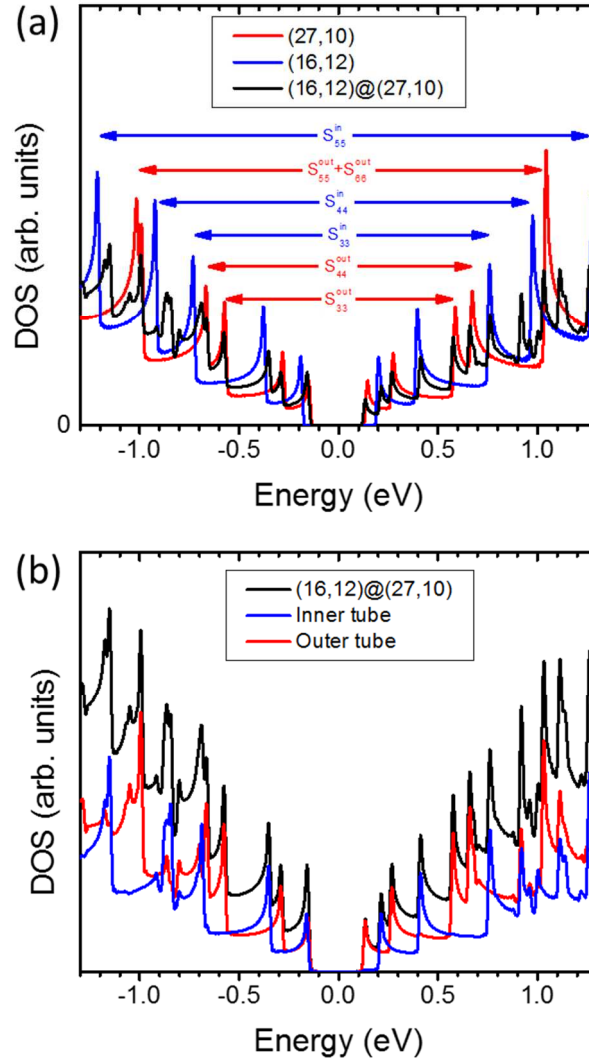


Figure 2: (a) The calculated DOS of the DWNT (16,12)@(27,10) (black line) in comparison with the calculated DOS of the non-interacting inner layer (16,12) (blue line) and outer layer (27,10) (red line). The horizontal arrows between the mirror spikes mark the optical transitions in the experimental energy range for the non-interacting layers, denoted by S_{ii}^{in} and S_{ii}^{out} for the inner and outer layer, respectively. (b) The calculated DOS of the DWNT (16,12)@(27,10) (black line) in comparison with the contributions of the inner layer (16,12) (blue line) and outer layer (27,10) (red line) are shown.

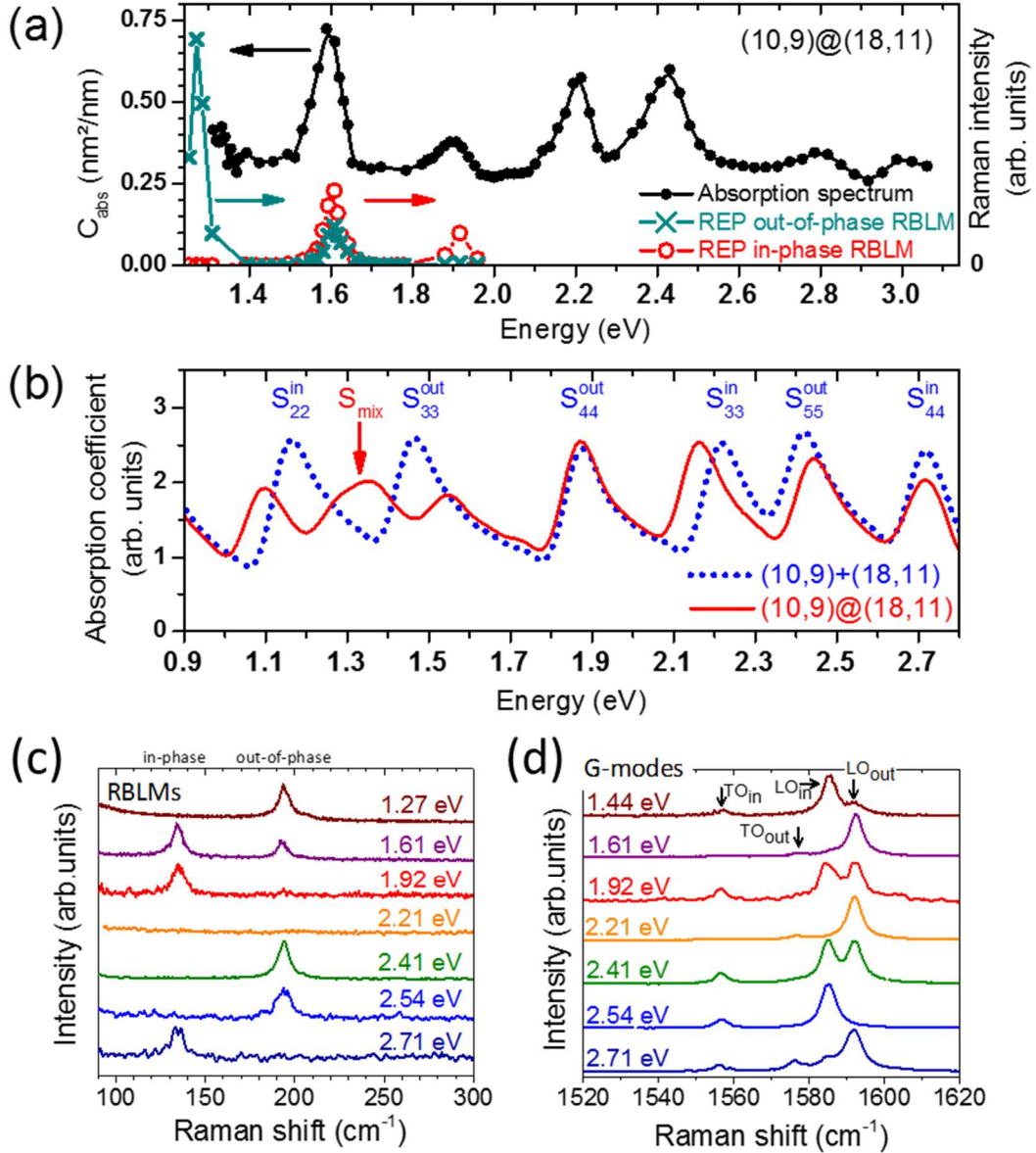


Figure 3: (a) Experimental absolute absorption cross-section spectra of the (10,9)@(18,11) DWNT for incident light polarization parallel to the DWNT axis, black dots and line (guide for eyes). Green (resp. red) open squares and line (guide for eyes), Raman excitation profiles of the out-of-phase (resp. in-phase) RBLM. (b) The calculated absorption coefficient of the (10,9)@(18,11) DWNT (red line) in comparison with that for a DWNT without interlayer interaction (dotted blue line). The blue S_{ii}^{in} and S_{ii}^{out} labels indicate the optical transitions of the inner and outer layers, respectively, the red arrow, labelled S_{mix} , points the new optical transition present only in the DWNT. Note that the energy scale of panel (b) has an offset of -340 meV relative to panel (a) in order to facilitate the direct comparison between experiment and theory, see main text. (c) and (d) Raman spectra of the individual free-standing (10,9)@(18,11) DWNT recorded with different excitations energies as labeled on the right hand sides: (c) RBLMs and (d) G-modes.

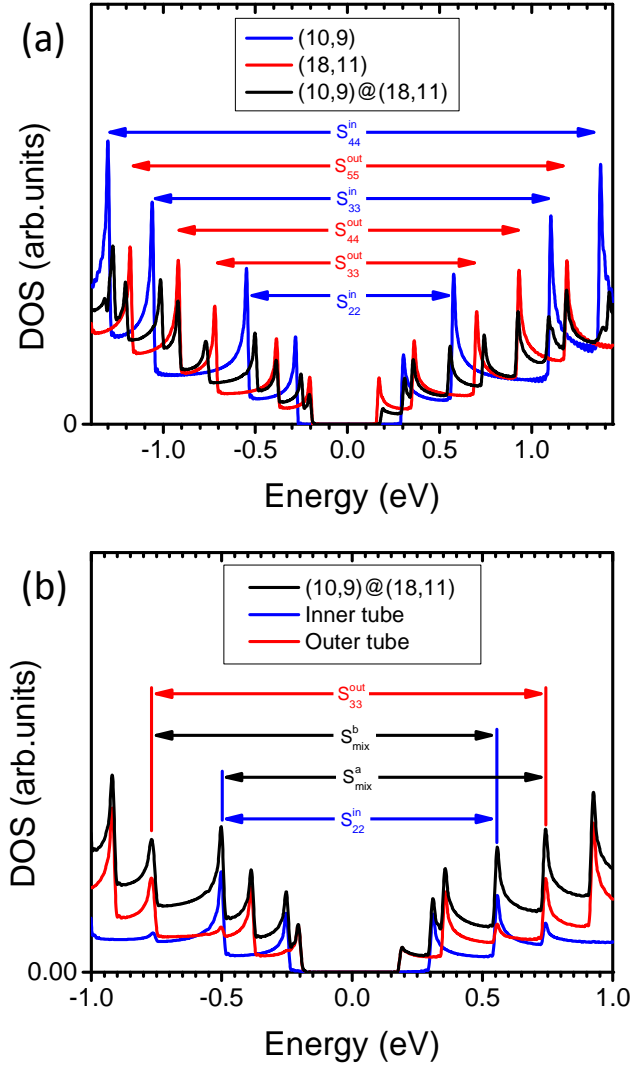


Figure 4: (a) The calculated DOS of the DWNT (10,9)@(18,11) (black line) in comparison with the calculated DOS of the non-interacting inner layer (10,9) (blue line) and outer layer (18,11) (red line). The horizontal arrows between the mirror spikes mark the optical transitions in the experimental energy range for the non-interacting layers, denoted by S_{ii}^{in} and S_{ii}^{out} for the inner and outer layer, respectively. (b) The calculated DOS of the DWNT (10,9)@(18,11) (black line) in comparison with the contributions of the inner layer (10,9) (blue line) and outer layer (18,11) (red line). The red and blue horizontal arrows show transitions between mirror spikes corresponding to specific pairs of transitions of the layers, while the black horizontal arrows show cross-band transitions, induced by the mixing of the electronic states.

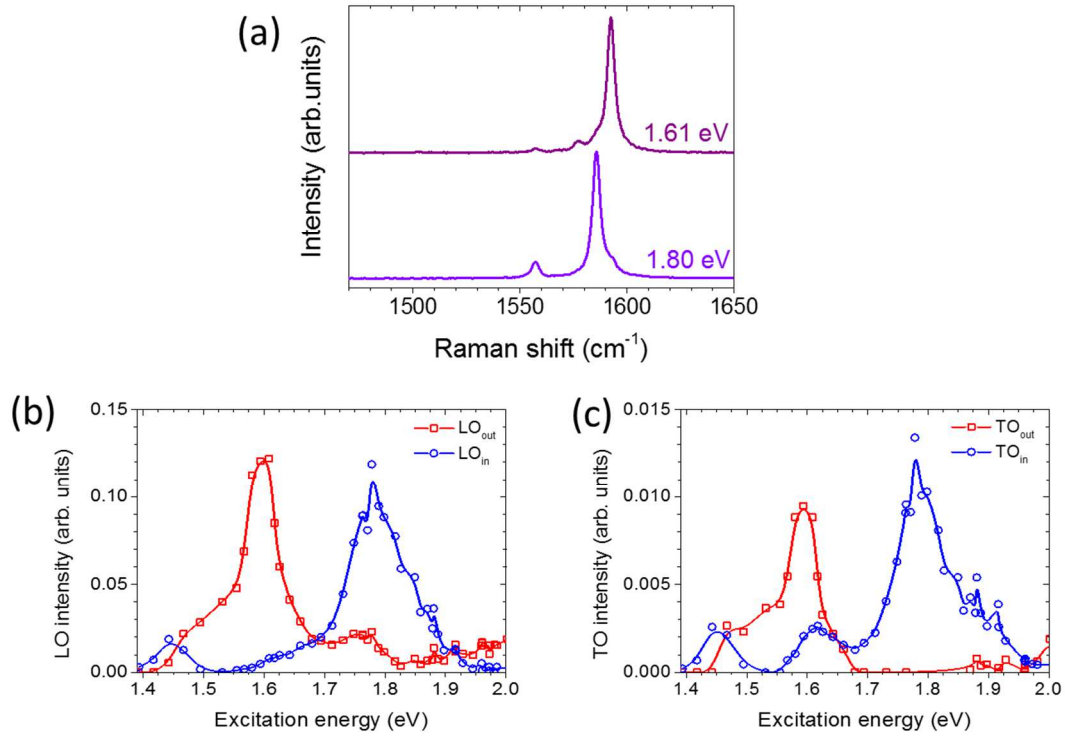


Figure 5: (a) Raman spectra of the (10,9)@(18,11) DWNT G-modes excited at 1.61 and 1.8 eV as labelled on the graph and corresponding to S_{mix} and $S_{mix}+E_{G-mode}$, respectively. (b) and (c) Raman Excitation Profiles of (10,9)@(18,11) DWNT G-modes of outer and inner layers, (a) LO modes and (b) TO modes.

Supplementary Information

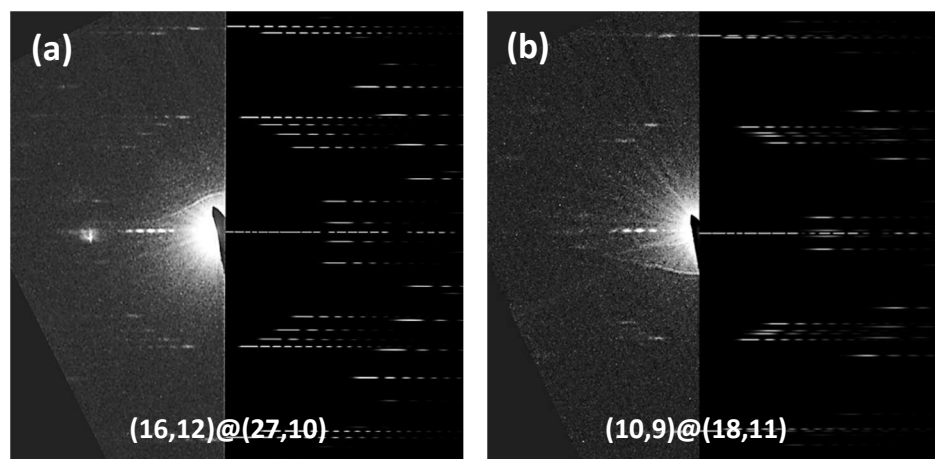


Figure S1: ED patterns, experimental (left part) and calculated (right part) of the DWNTs (a) (16,12)@(27,10) and (b) (10,9)@(18,11).

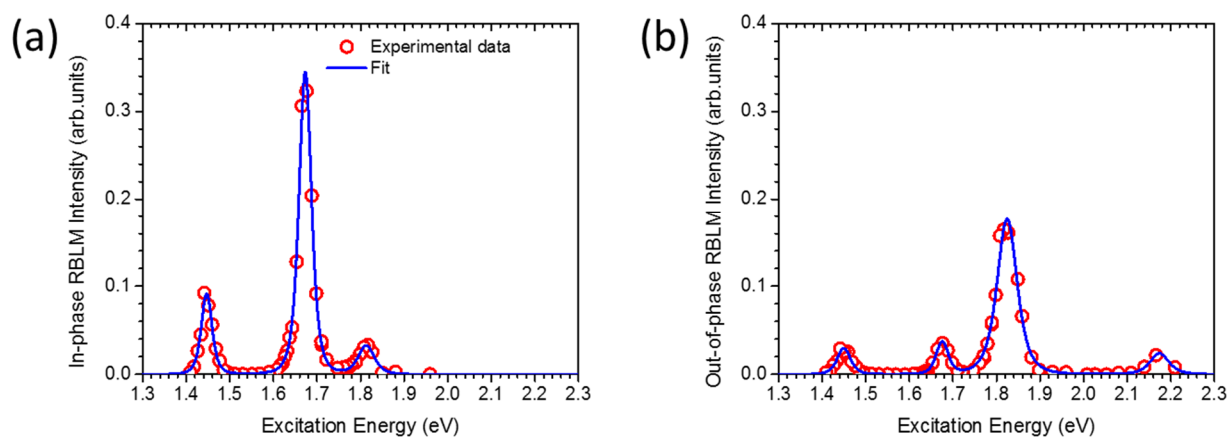


Figure S2: Raman excitation profiles of the in-phase RBLM (a) and out-of-phase RBLM (b) on the (16,12)@(27,10) DWNT. Red open dots, experimental data and solid blue line, fit. See Ref. [S1].

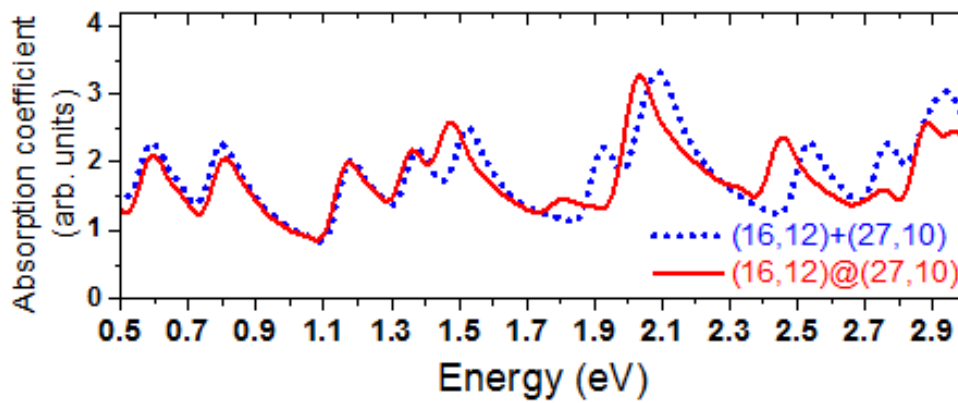


Figure S3: The calculated absorption coefficient of the (16,12)@(27,10) DWNT (red line) in comparison with that for a DWNT without interlayer interaction (dotted blue line).

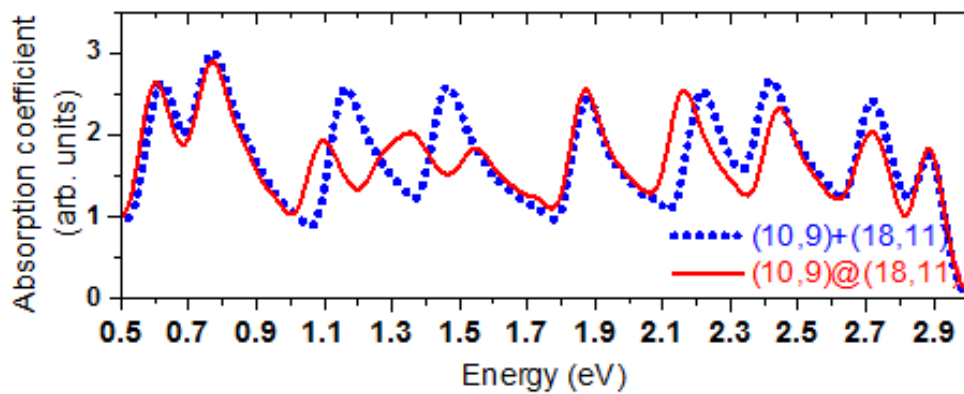


Figure S4: The calculated absorption coefficient of the (10,9)@(18,11) DWNT (red line) in comparison with that for a DWNT without interlayer interaction (dotted blue line).

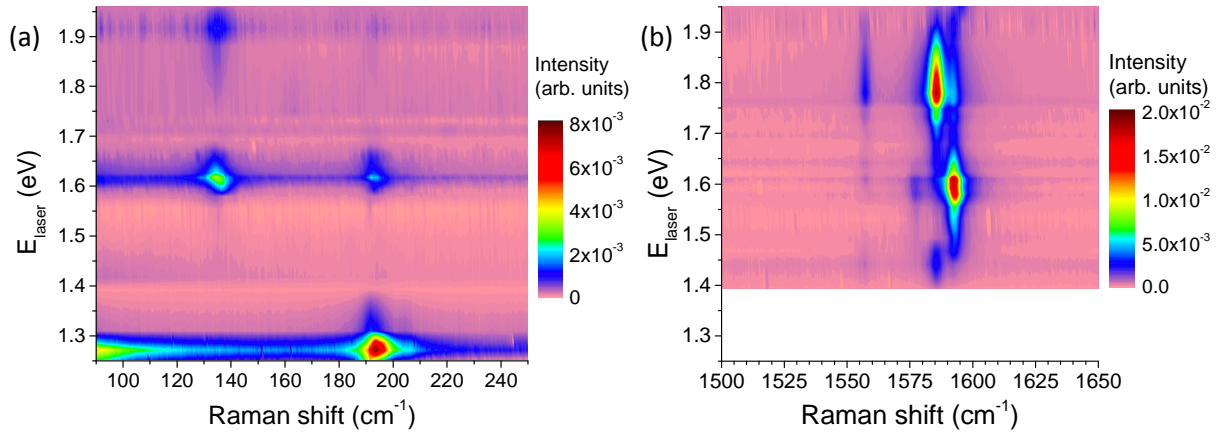


Figure S5: Raman maps of (a) RBLM and (b) G-modes of (10,9)@(18,11) as function of excitation energy in the range 1.25 – 1.95 eV.

Optical transition	Experimental transition energy (eV)			Calculated transition energy (eV)		
	(16,12)@(27,10)	(16,12)	(27,10)	(16,12)@(27,10)	(16,12)	(27,10)
S_{33}^{out}	1.44		1.51	1.14		1.15
S_{44}^{out}	1.67		1.72	1.34		1.33
S_{33}^{in}	1.81	1.885		1.44	1.49	
S_{44}^{in}	2.15	2.34		1.76	1.89	
$S_{55}^{out} + S_{66}^{out}$	2.44			1.985		2.035
S_{55}^{in}	2.76	2.895	2.485	2.4	2.48	

Table S1: Energy of the optical transitions of the (16,12)@(27,10) DWNT, (16,12) and (27,10) SWNTs as determined from experiments and theory. All data are from this work, except the experimental data of the (16,12) and (27,10) SWNTs which are extracted from Ref. [S2].

Optical transition	Experimental transition energy (eV)			Calculated transition energy (eV)		
	(10,9)@(18,11)	(10,9)	(18,11)	(10,9)@(18,11)	(10,9)	(18,11)
S_{22}^{in}	1.26	1.395		1.04	1.12	
S_{mix}	1.59			1.265		
S_{33}^{out}	1.89		1.805	1.49		1.41
S_{44}^{out}	2.2		2.29	1.83		1.84
S_{33}^{in}	2.42	2.565		2.09	2.16	
S_{55}^{out}	2.79		2.78	2.37		2.36
S_{44}^{in}	2.99	3.05		2.68	2.67	

Table S2: Energy of the optical transitions of the (10,9)@(18,11) DWNT, (10,9) and (18,11) SWNTs as determined from experiments and theory. All data are from this work, except the experimental data of the (10,9) and (18,11) SWNTs which are extracted from Ref. [S2].

References

[S1] Tran, H. N.; Blancon, J. C.; Arenal, R.; Parret, R.; Zahab, A. A.; Ayari, A.; Vallée, F.; Del Fatti, N.; Sauvajol, J. L. ; Paillet, M. Quantum interference effects on the intensity of the G modes in double-walled carbon nanotubes. *Phys. Rev. B* **2017**, 95, 205411.

[S2] Liu, K.; Deslippe, J.; Xiao, F.; Capaz, R. B.; Hong, X.; Aloni, S.; Zettl, A.; Wang, W.; Bai, X.; Louie, S. G.; Wang, E.; Wang, F. An atlas of carbon nanotube optical transitions. *Nat. Nanotechnol.* **2012**, 7, 325–329.